ENM 540: Data-driven modeling and probabilistic scientific computing

Lecture #10: Deep learning applications

Paris Perdikaris
February 15, 2018

UNIVERSITY of PENNSYLVANIA

Deep learning: History and recent success

Applications of machine learning. Machine learning is having a substantial effect on many areas of technology and science; examples of recent applied success stories include robotics and autonomous vehicle control (top left), speech processing and natural language processing (top left), neuroscience research (middle), and applications in computer vision (top right).

Jordan, M. I., & Mitchell, T. M. (2015). Machine learning: Trends, perspectives, and prospects. Science, 349(6245), 255-260.

Deep learning: History and recent success

Deep learning: History and recent success

- 1940s - Neural networks were proposed
- 1960s - Deep neural networks were proposed
- 1989 - Neural networks for recognizing digits (LeNet)
- 1990s - Hardware for shallow neural nets (Intel ETANN)
- 2011 - Breakthrough DNN-based speech recognition (Microsoft)
- 2012 - DNNs for vision start supplanting hand-crafted approaches (AlexNet)
- 2014+ - Rise of DNN accelerator research (Neuflow, DianNao...)

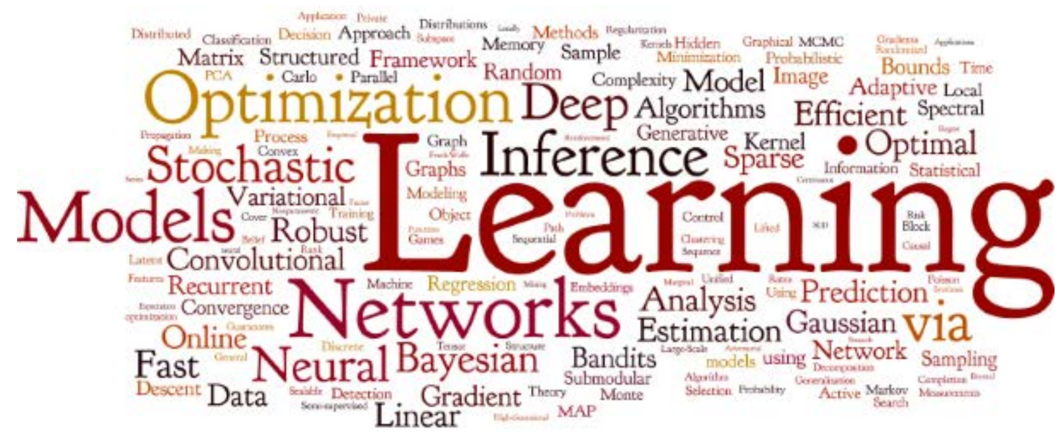

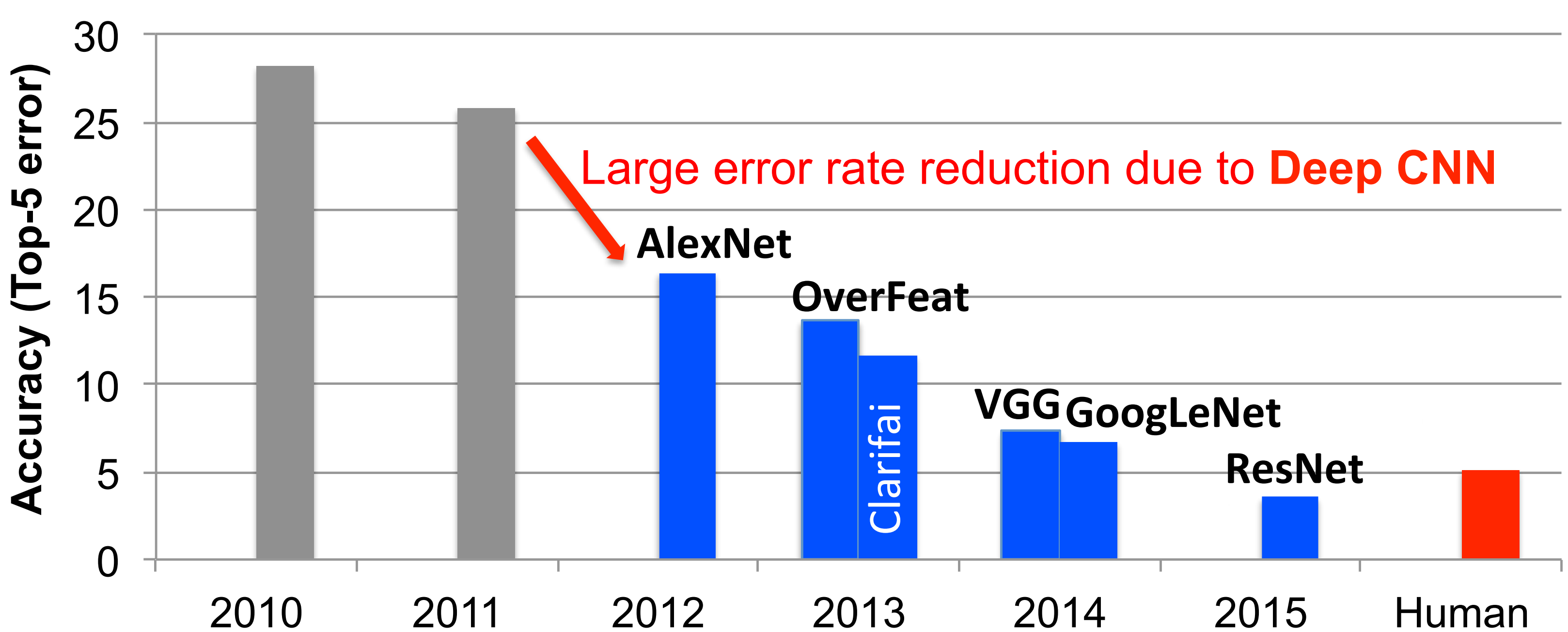

In 2015, the ImageNet winning entry, ResNet, exceeded human-level accuracy with a top-5 error rate below 5%.

Since then, the error rate has dropped below 3% and more focus is now being placed on more challenging components of the competition, such as object detection and localization.

Image super-resolution

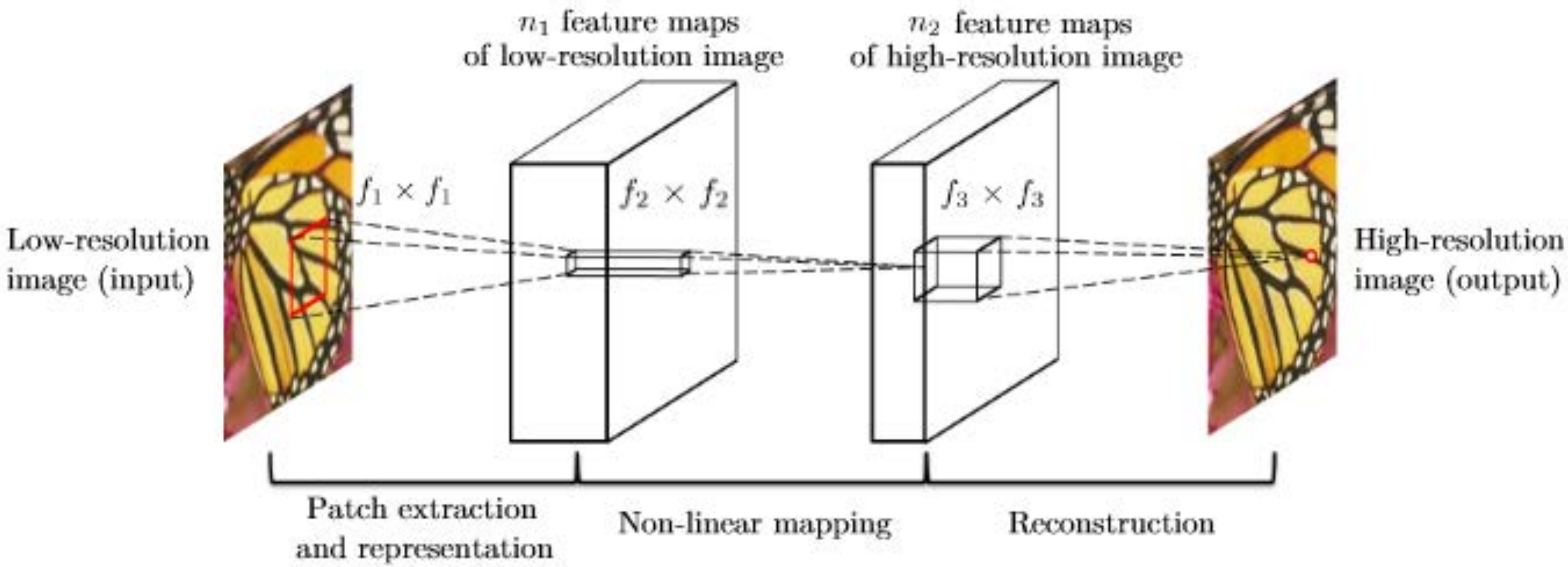

Fig. 2. Given a low-resolution image $\mathbf{Y}$, the first convolutional layer of the SRCNN extracts a set of feature maps. The second layer maps these feature maps nonlinearly to high-resolution patch representations. The last layer combines the predictions within a spatial neighbourhood to produce the final high-resolution image $F(\mathbf{Y})$.

Dong, C., Loy, C. C., He, K., & Tang, X. (2014, September). Learning a deep convolutional network for image super-resolution. In European Conference on Computer Vision (pp. 184-199). Springer, Cham.

Transfer learning

Source

Refs (”restaurant night”)

Ours

Source

Refs (”building beach”)

Ours

https://news.developer.nvidia.com/style-transfer-from-multiple-reference-images/

Modeling long-term dependencies in sequence data

For $\bigoplus_{n=1,\dots,m}$ where $\mathcal{L}_{m_\bullet} = 0$, hence we can find a closed subset $\mathcal{H}$ in $\mathcal{H}$ and any sets $\mathcal{F}$ on X, U is a closed immersion of S, then $U \to T$ is a separated algebraic space.

Proof. Proof of (1). It also start we get

$$S = \mathrm{Spec}(R) = U \times_X U \times_X U$$

and the comparicoly in the fibre product covering we have to prove the lemma generated by $\coprod Z \times_U U \to V$. Consider the maps M along the set of points Sch_{fppf} and $U \to U$ is the fibre category of S in U in Section, ?? and the fact that any U affine, see Morphisms, Lemma ??. Hence we obtain a scheme S and any open subset $W \subset U$ in $Sh(G)$ such that $\mathrm{Spec}(R') \to S$ is smooth or an

$$U = \bigcup U_i \times_{S_i} U_i$$

which has a nonzero morphism we may assume that f_i is of finite presentation over S. We claim that $\mathcal{O}_{X,x}$ is a scheme where $x, x', s'' \in S'$ such that $\mathcal{O}_{X,x'} \to \mathcal{O}'_{X',x'}$ is separated. By Algebra, Lemma ?? we can define a map of complexes $\mathrm{GL}_{S'}(x'/S'')$ and we win. □

To prove study we see that $\mathcal{F}|_U$ is a covering of $\mathcal{X}'$, and $\mathcal{T}_i$ is an object of $\mathcal{F}_{X/S}$ for $i > 0$ and $\mathcal{F}_p$ exists and let $\mathcal{F}_i$ be a presheaf of $\mathcal{O}_X$-modules on $\mathcal{C}$ as a $\mathcal{F}$-module. In particular $\mathcal{F} = U/\mathcal{F}$ we have to show that

$$\widetilde{M}^\bullet = \mathcal{I}^\bullet \otimes_{\mathrm{Spec}(k)} \mathcal{O}_{S,s} - i_X^{-1}\mathcal{F})$$

is a unique morphism of algebraic stacks. Note that

$$\mathrm{Arrows} = (Sch/S)^{opp}_{fppf}, (Sch/S)_{fppf}$$

and

$$V = \Gamma(S, \mathcal{O}) \longmapsto (U, \mathrm{Spec}(A))$$

is an open subset of X. Thus U is affine. This is a continuous map of X is the inverse, the groupoid scheme S.

Proof. See discussion of sheaves of sets. □

The result for prove any open covering follows from the less of Example ??. It may replace S by $X_{spaces,étale}$ which gives an open subspace of X and T equal to S_{Zar}, see Descent, Lemma ??. Namely, by Lemma ?? we see that R is geometrically regular over S.

Lemma 0.1. *Assume (3) and (3) by the construction in the description.*

Suppose $X = \lim |X|$ (by the formal open covering X and a single map $\underline{Proj}_X(\mathcal{A}) = \mathrm{Spec}(B)$ over U compatible with the complex

$$Set(\mathcal{A}) = \Gamma(X, \mathcal{O}_{X,\mathcal{O}_X}).$$

When in this case of to show that $\mathcal{Q} \to \mathcal{C}_{Z/X}$ is stable under the following result in the second conditions of (1), and (3). This finishes the proof. By Definition ?? (without element is when the closed subschemes are catenary. If T is surjective we may assume that T is connected with residue fields of S. Moreover there exists a closed subspace $Z \subset X$ of X where U in X' is proper (some defining as a closed subset of the uniqueness it suffices to check the fact that the following theorem

(1) *f is locally of finite type. Since $S = \mathrm{Spec}(R)$ and $Y = \mathrm{Spec}(R)$.*

Proof. This is form all sheaves of sheaves on X. But given a scheme U and a surjective étale morphism $U \to X$. Let $U \cap U = \coprod_{i=1,\dots,n} U_i$ be the scheme X over S at the schemes $X_i \to X$ and $U = \lim_i X_i$. □

The following lemma surjective restrocomposes of this implies that $\mathcal{F}_{x_0} = \mathcal{F}_{x_0} = \mathcal{F}_{\mathcal{X},\dots,0}$.

Lemma 0.2. *Let X be a locally Noetherian scheme over S, $E = \mathcal{F}_{X/S}$. Set $\mathcal{I} = \mathcal{J}_1 \subset \mathcal{I}'_n$. Since $\mathcal{I}^n \subset \mathcal{I}^n$ are nonzero over $i_0 \leq \mathfrak{p}$ is a subset of $\mathcal{J}_{n,0} \circ \overline{A}_2$ works.*

Lemma 0.3. *In Situation ??. Hence we may assume $\mathfrak{q}' = 0$.*

Proof. We will use the property we see that $\mathfrak{p}$ is the mext functor (??). On the other hand, by Lemma ?? we see that

$$D(\mathcal{O}_{X'}) = \mathcal{O}_X(D)$$

where K is an F-algebra where δ_{n+1} is a scheme over S. □

Example: Text generation with LSTMs

http://karpathy.github.io/2015/05/21/rnn-effectiveness/

Modeling long-term dependencies in sequence data

Proof. Omitted. □

Lemma 0.1. *Let $\mathcal{C}$ be a set of the construction.*

Let $\mathcal{C}$ be a gerber covering. Let $\mathcal{F}$ be a quasi-coherent sheaves of $\mathcal{O}$-modules. We have to show that

$$\mathcal{O}_{\mathcal{O}_X} = \mathcal{O}_X(\mathcal{L})$$

.

Proof. This is an algebraic space with the composition of sheaves $\mathcal{F}$ on $X_{\acute{e}tale}$ we have

$$\mathcal{O}_X(\mathcal{F}) = \{morph_1 \times_{\mathcal{O}_X} (\mathcal{G}, \mathcal{F})\}$$

where $\mathcal{G}$ defines an isomorphism $\mathcal{F} \to \mathcal{F}$ of $\mathcal{O}$-modules. □

Lemma 0.2. *This is an integer $\mathcal{Z}$ is injective.*

Proof. See Spaces, Lemma ??. □

Lemma 0.3. *Let S be a scheme. Let X be a scheme and X is an affine open covering. Let $\mathcal{U} \subset \mathcal{X}$ be a canonical and locally of finite type. Let X be a scheme. Let X be a scheme which is equal to the formal complex.*

The following to the construction of the lemma follows.

Let X be a scheme. Let X be a scheme covering. Let

$$b : X \to Y' \to Y \to Y \to Y' \times_X Y \to X.$$

be a morphism of algebraic spaces over S and Y.

Proof. Let X be a nonzero scheme of X. Let X be an algebraic space. Let $\mathcal{F}$ be a quasi-coherent sheaf of $\mathcal{O}_X$-modules. The following are equivalent

(1) $\mathcal{F}$ is an algebraic space over S.
(2) If X is an affine open covering.

Consider a common structure on X and X the functor $\mathcal{O}_X(U)$ which is locally of finite type. □

This since $\mathcal{F} \in \mathcal{F}$ and $x \in \mathcal{G}$ the diagram

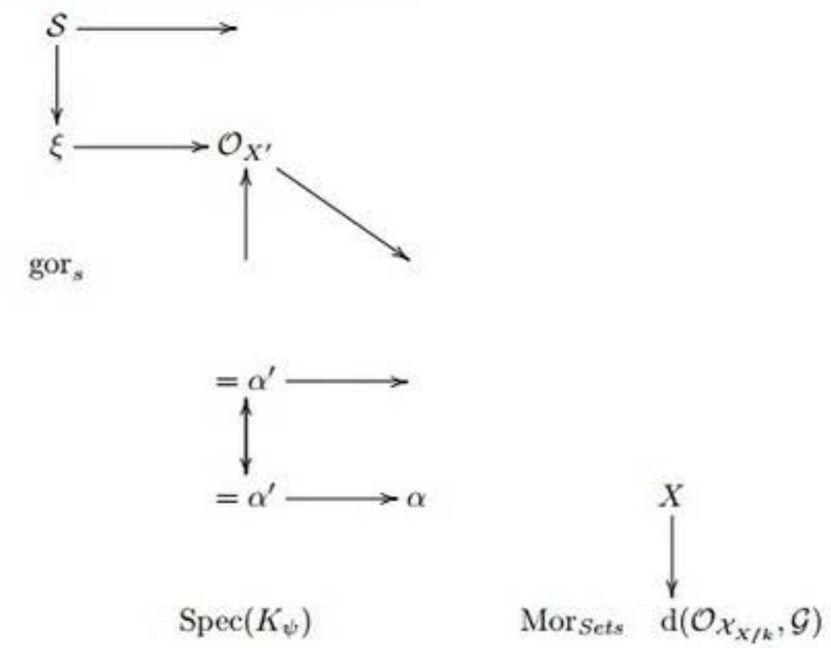

is a limit. Then $\mathcal{G}$ is a finite type and assume S is a flat and $\mathcal{F}$ and $\mathcal{G}$ is a finite type f_*. This is of finite type diagrams, and

- the composition of $\mathcal{G}$ is a regular sequence,
- $\mathcal{O}_{X'}$ is a sheaf of rings.

□

Proof. We have see that $X = \mathrm{Spec}(R)$ and $\mathcal{F}$ is a finite type representable by algebraic space. The property $\mathcal{F}$ is a finite morphism of algebraic stacks. Then the cohomology of X is an open neighbourhood of U. □

Proof. This is clear that $\mathcal{G}$ is a finite presentation, see Lemmas ??.
A *reduced above* we conclude that U is an open covering of $\mathcal{C}$. The functor $\mathcal{F}$ is a "field

$$\mathcal{O}_{X,x} \longrightarrow \mathcal{F}_{\overline{x}} \quad \text{-}1(\mathcal{O}_{X_{\acute{e}tale}}) \longrightarrow \mathcal{O}_{X_\ell}^{-1}\mathcal{O}_{X_\lambda}(\mathcal{O}_{X_\eta}^{\overline{v}})$$

is an isomorphism of covering of $\mathcal{O}_{X_i}$. If $\mathcal{F}$ is the unique element of $\mathcal{F}$ such that X is an isomorphism.
The property $\mathcal{F}$ is a disjoint union of Proposition ?? and we can filtered set of presentations of a scheme $\mathcal{O}_X$-algebra with $\mathcal{F}$ are opens of finite type over S.
If $\mathcal{F}$ is a scheme theoretic image points. □

If $\mathcal{F}$ is a finite direct sum $\mathcal{O}_{X_\lambda}$ is a closed immersion, see Lemma ??. This is a sequence of $\mathcal{F}$ is a similar morphism.

Example: Text generation with LSTMs

http://karpathy.github.io/2015/05/21/rnn-effectiveness/

Attention and captioning

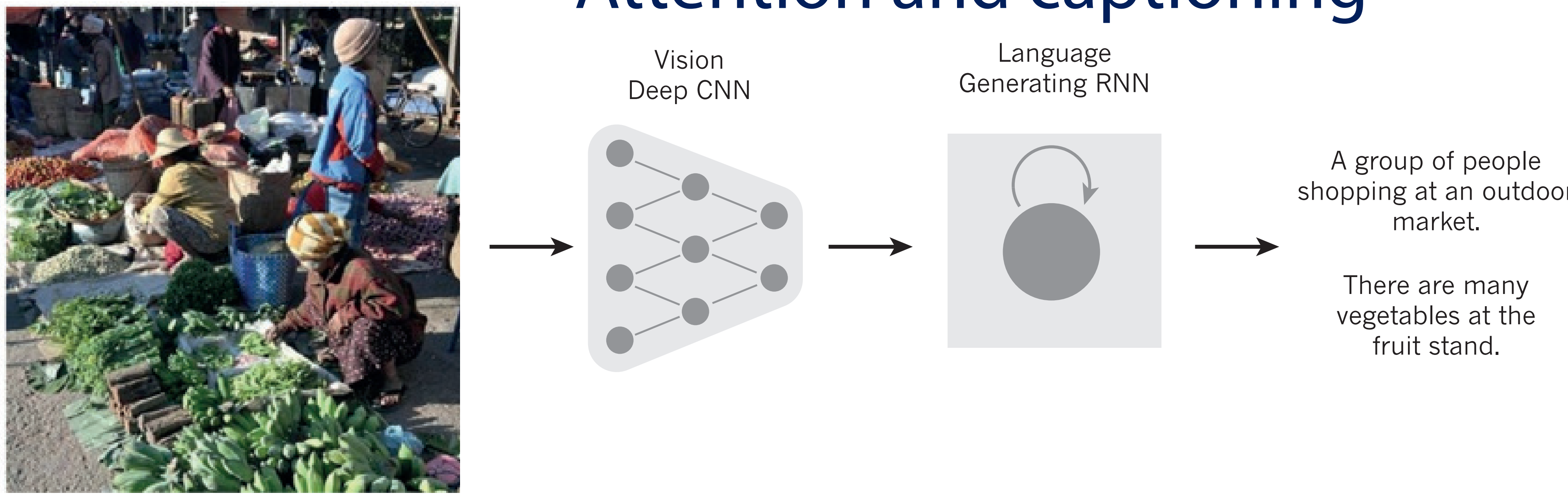

A woman is throwing a **frisbee** in a park.

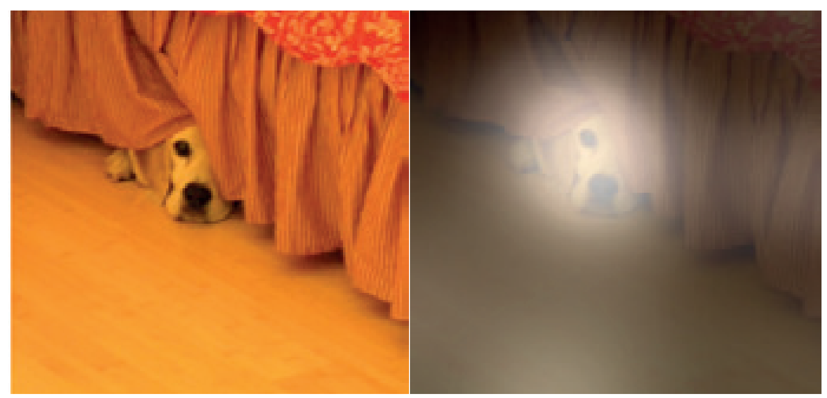

A **dog** is standing on a hardwood floor.

A **stop** sign is on a road with a mountain in the background

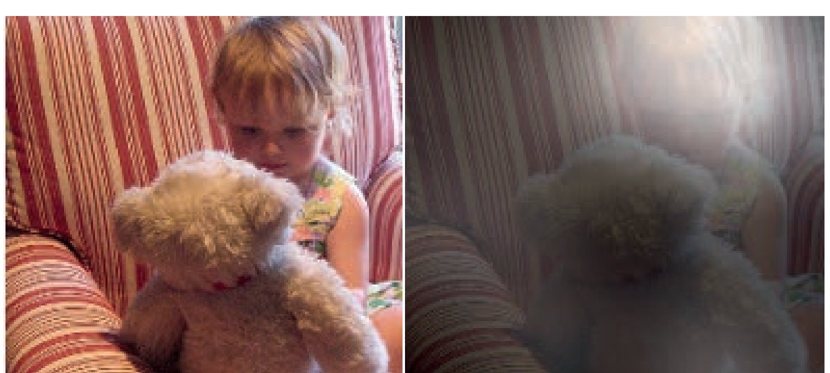

A little **girl** sitting on a bed with a teddy bear.

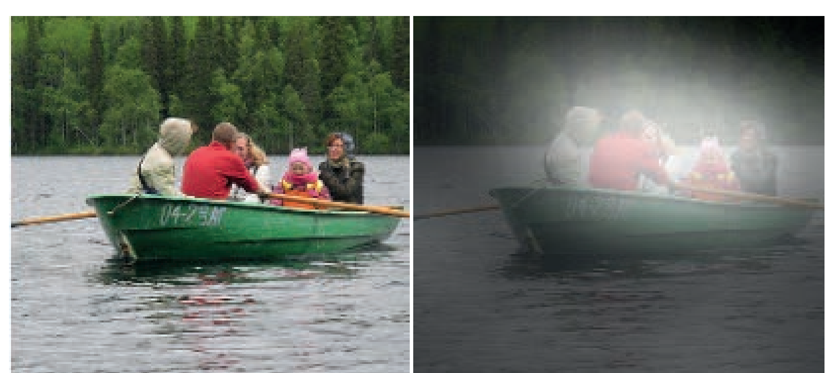

A group of **people** sitting on a boat in the water.

A giraffe standing in a forest with **trees** in the background.

LeCun, Y., Bengio, Y., & Hinton, G. (2015). Deep learning. Nature, 521(7553), 436.

Object segmentation and tracking

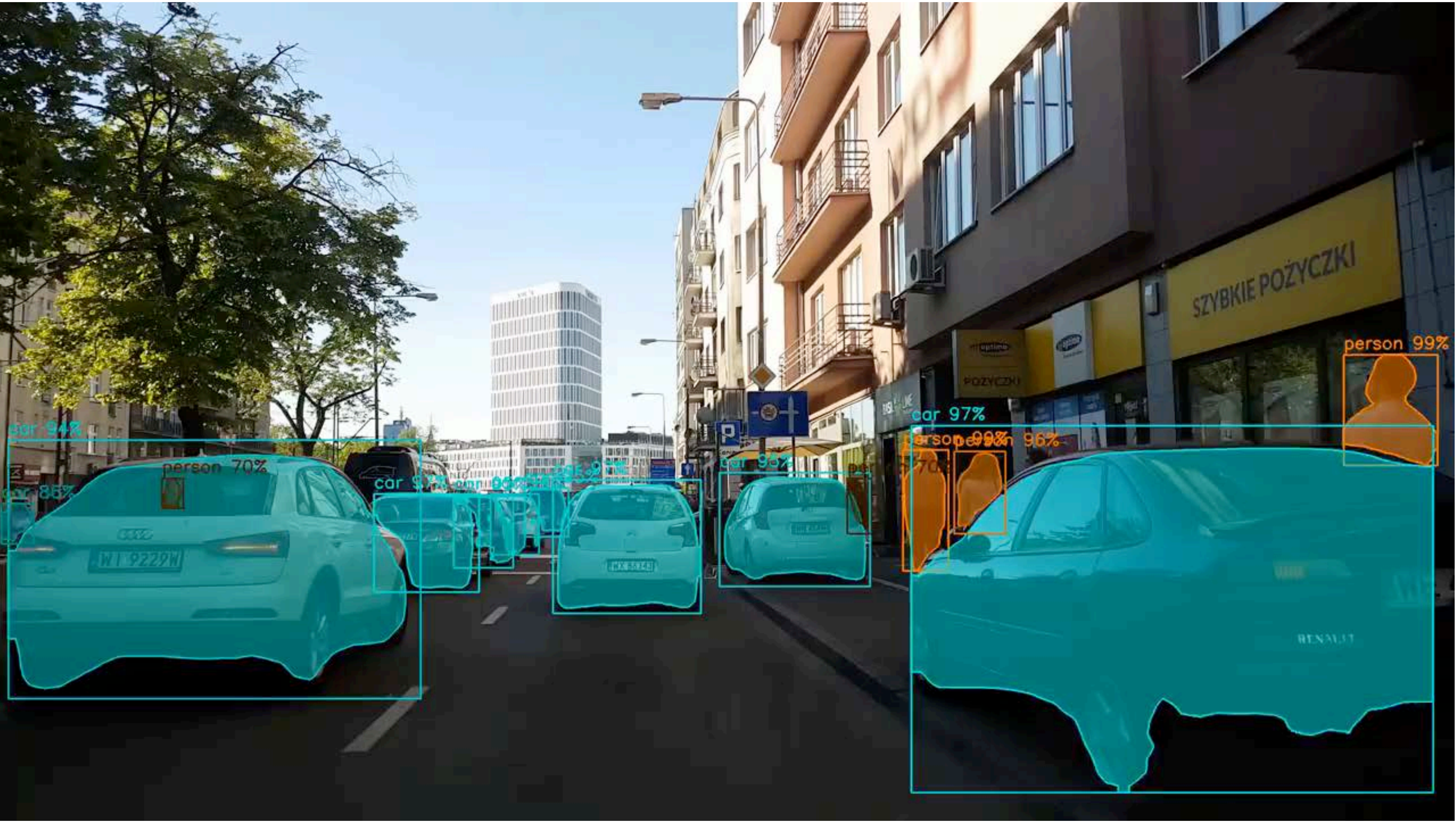

He, K., Gkioxari, G., Dollár, P., & Girshick, R. (2017, October). Mask r-cnn. 2017 IEEE International Conference on Computer Vision (ICCV).

Systems identification (ODEs)

$$\frac{d}{dt}\boldsymbol{x}(t) = \boldsymbol{f}\left(\boldsymbol{x}(t)\right)$$

Harmonic Oscillator:

$$\dot{x} = -0.1\ x^3 + 2.0\ y^3$$
$$\dot{y} = -2.0\ x^3 - 0.1\ y^3$$

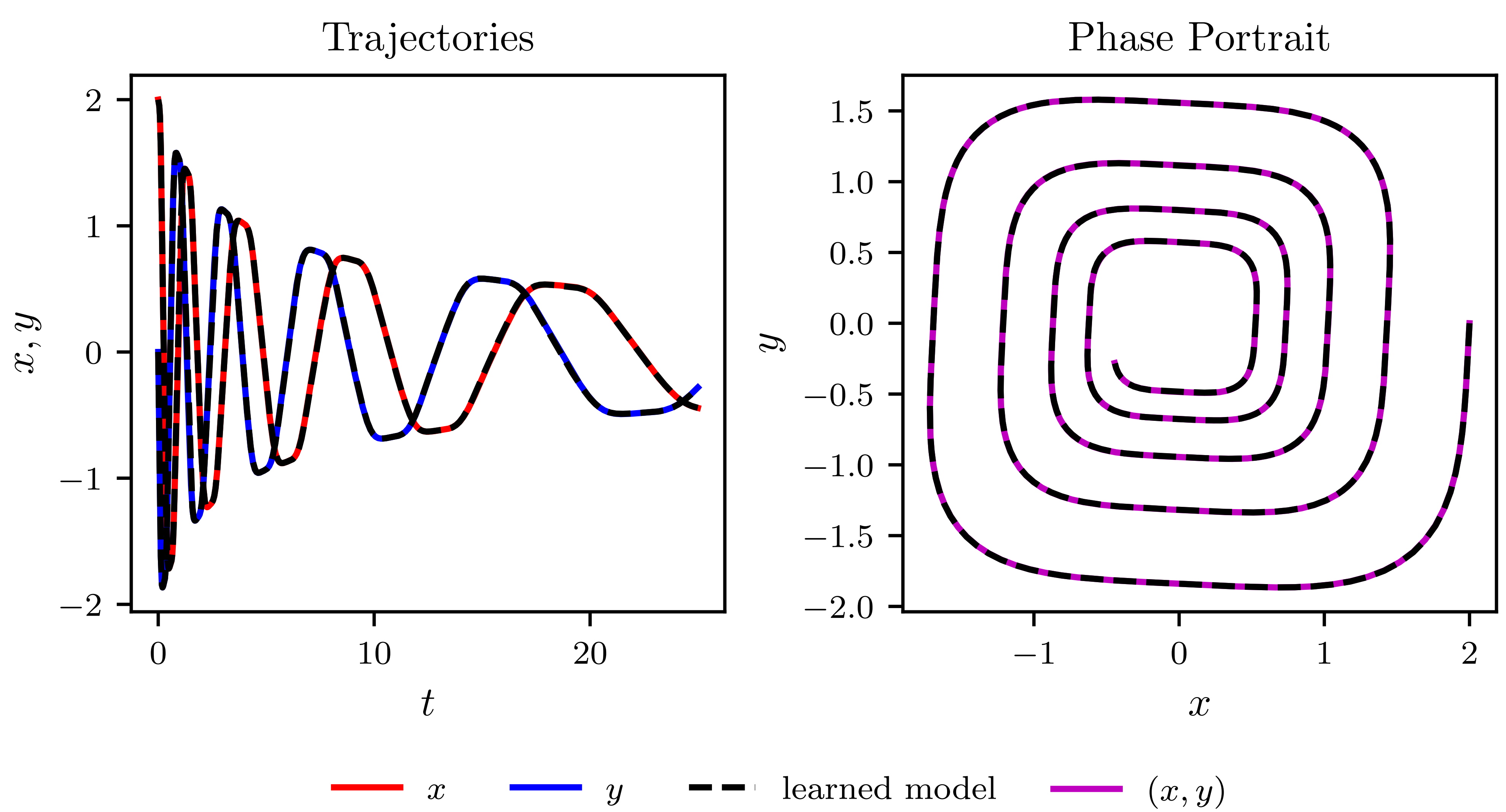

Raissi, M., Perdikaris, P., & Karniadakis, G. E. (2018). Multistep Neural Networks for Data-driven Discovery of Nonlinear Dynamical Systems. arXiv preprint

Systems identification (ODEs)

Lorenz System:

$$\dot{x} = 10(y - x),$$
$$\dot{y} = x(28 - z) - y,$$
$$\dot{z} = xy - (8/3)z.$$

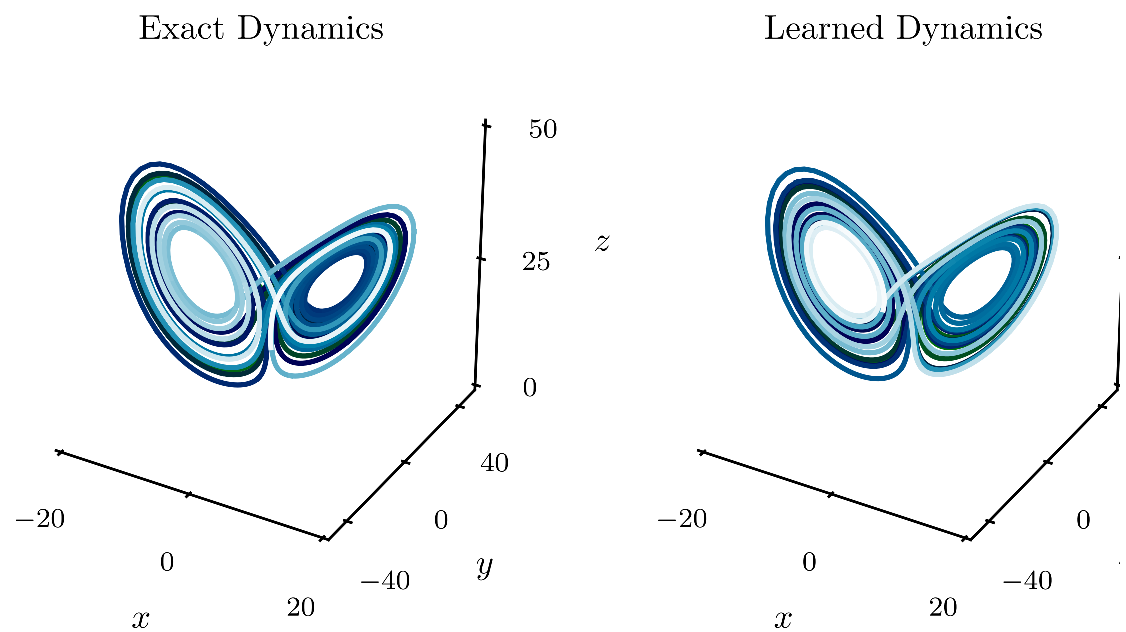

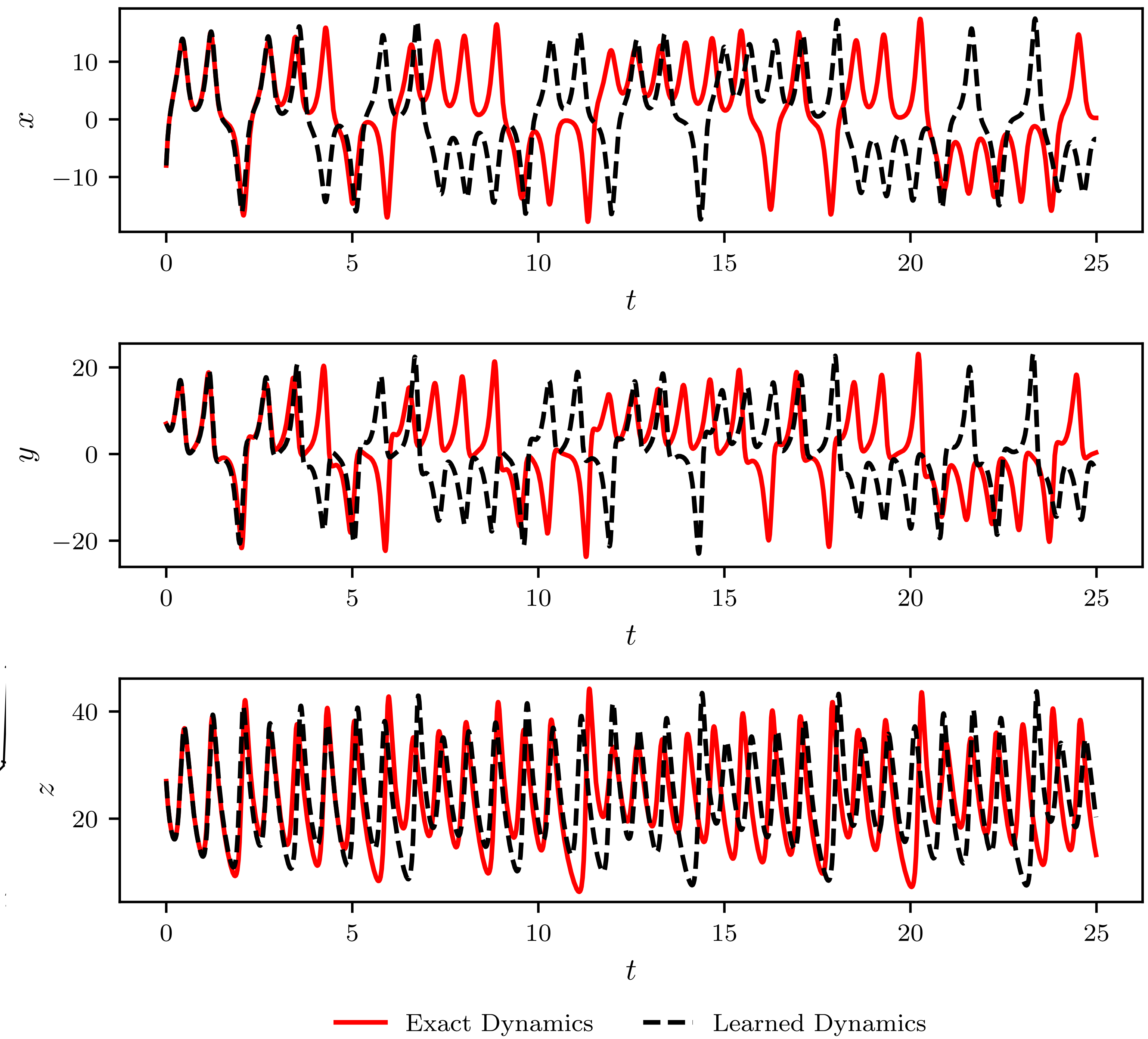

Raissi, M., Perdikaris, P., & Karniadakis, G. E. (2018). Multistep Neural Networks for Data-driven Discovery of Nonlinear Dynamical Systems. arXiv preprint

Systems identification (PDEs)

$$u_t = \mathcal{N}(t, x, u, u_x, u_{xx}, \ldots)$$

Example:

The KdV equation:

$$u_t = -uu_x - u_{xxx}$$

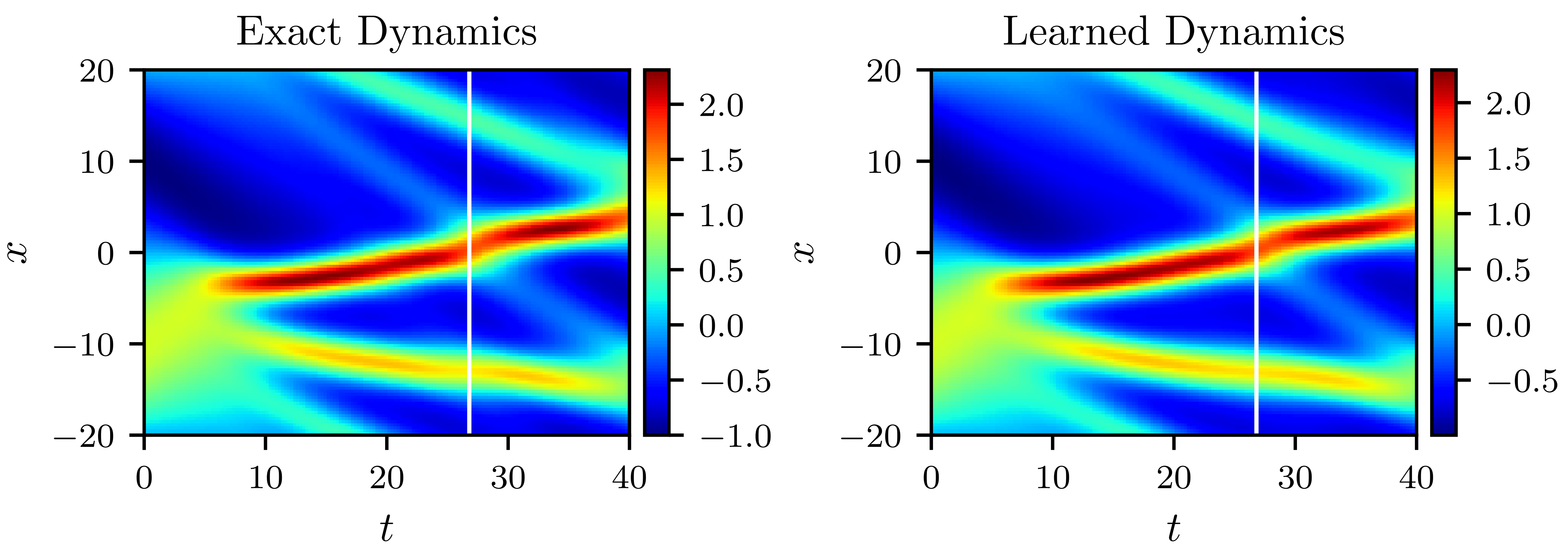

Raissi, M. (2018). Deep Hidden Physics Models: Deep Learning of Nonlinear Partial Differential Equations. arXiv preprint arXiv:1801.06637.

Systems identification (PDEs)

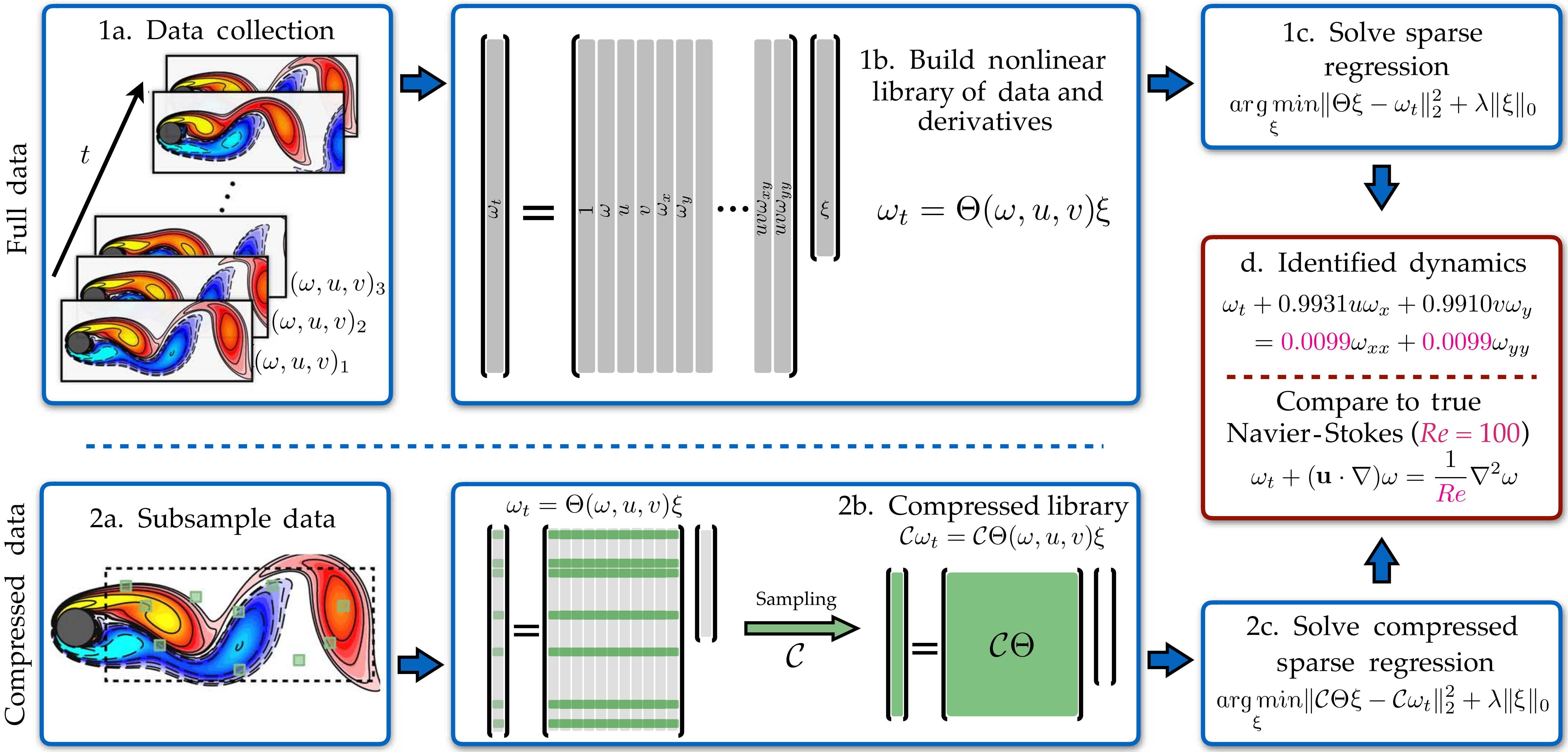

Fig. 1. Steps in the PDE functional identification of nonlinear dynamics (PDE-FIND) algorithm, applied to infer the Navier-Stokes equations from data. (1a) Data are collected as snapshots of a solution to a PDE. (1b) Numerical derivatives are taken, and data are compiled into a large matrix $\mathbf{\Theta}$, incorporating candidate terms for the PDE. (1c) Sparse regressions are used to identify active terms in the PDE. (2a) For large data sets, sparse sampling may be used to reduce the size of the problem. (2b) Subsampling the data set is equivalent to taking a subset of rows from the linear system in Eq. 2. (2c) An identical sparse regression problem is formed but with fewer rows. (d) Active terms in ξ are synthesized into a PDE.

Rudy, S. H., Brunton, S. L., Proctor, J. L., & Kutz, J. N. (2017). Data-driven discovery of partial differential equations. Science Advances, 3(4), e1602614.

Diagnosing Pneumonia at Radiologist-Level Accuracy

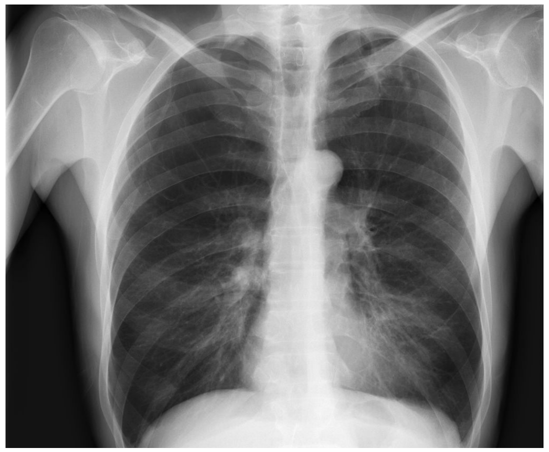

Input
Chest X-Ray Image

CheXNet
121-layer CNN

Output
Pneumonia Positive (85%)

Abstract

We develop an algorithm that can detect pneumonia from chest X-rays at a level exceeding practicing radiologists. Our algorithm, CheXNet, is a 121-layer convolutional neural network trained on ChestX-ray14, currently the largest publicly available chest X-ray dataset, containing over 100,000 frontal-view X-ray images with 14 diseases. Four practicing academic radiologists annotate a test set, on which we compare the performance of CheXNet to that of radiologists. We find that CheXNet exceeds average radiologist performance on the F1 metric. We extend CheXNet to detect all 14 diseases in ChestX-ray14 and achieve state of the art results on all 14 diseases.

	F1 Score (95% CI)
Radiologist 1	0.383 (0.309, 0.453)
Radiologist 2	0.356 (0.282, 0.428)
Radiologist 3	0.365 (0.291, 0.435)
Radiologist 4	0.442 (0.390, 0.492)
Radiologist Avg.	0.387 (0.330, 0.442)
CheXNet	0.435 (0.387, 0.481)

Rajpurkar, P., Irvin, J., Zhu, K., Yang, B., Mehta, H., Duan, T., ... & Lungren, M. P. (2017). CheXNet: Radiologist-Level Pneumonia Detection on Chest X-Rays with Deep Learning. arXiv preprint

Arrhythmia Detection with ConvNets

Abstract

We develop an algorithm which exceeds the performance of board certified cardiologists in detecting a wide range of heart arrhythmias from electrocardiograms recorded with a single-lead wearable monitor. We build a dataset with more than 500 times the number of unique patients than previously studied corpora. On this dataset, we train a 34-layer convolutional neural network which maps a sequence of ECG samples to a sequence of rhythm classes. Committees of board-certified cardiologists annotate a gold standard test set on which we compare the performance of our model to that of 6 other individual cardiologists. We exceed the average cardiologist performance in both recall (sensitivity) and precision (positive predictive value).

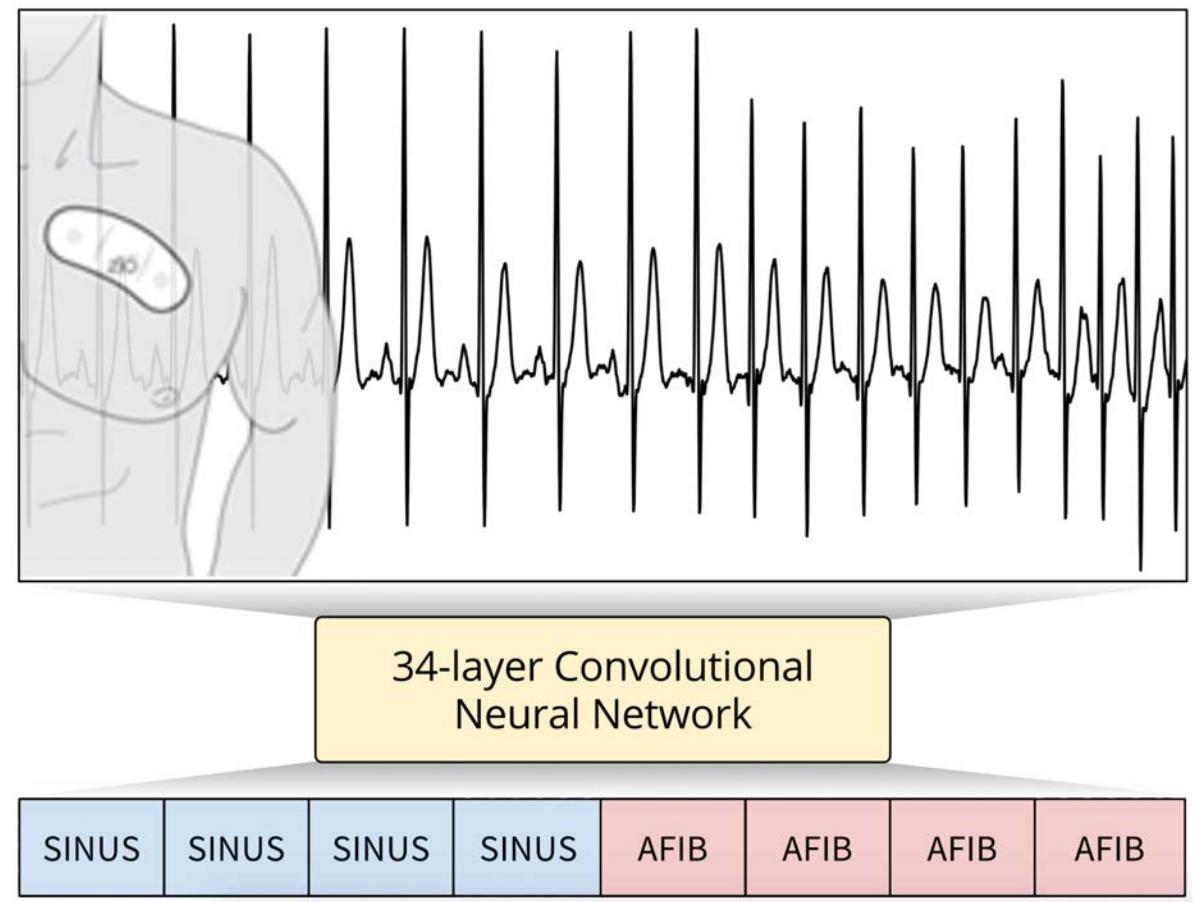

Figure 1. Our trained convolutional neural network correctly detecting the sinus rhythm (SINUS) and Atrial Fibrillation (AFIB) from this ECG recorded with a single-lead wearable heart monitor.

Rajpurkar, P., Hannun, A. Y., Haghpanahi, M., Bourn, C., & Ng, A. Y. (2017). Cardiologist-level arrhythmia detection with convolutional neural networks. arXiv preprint arXiv:1707.01836.

Reducing the Risk of Second Breast Cancer Surgery

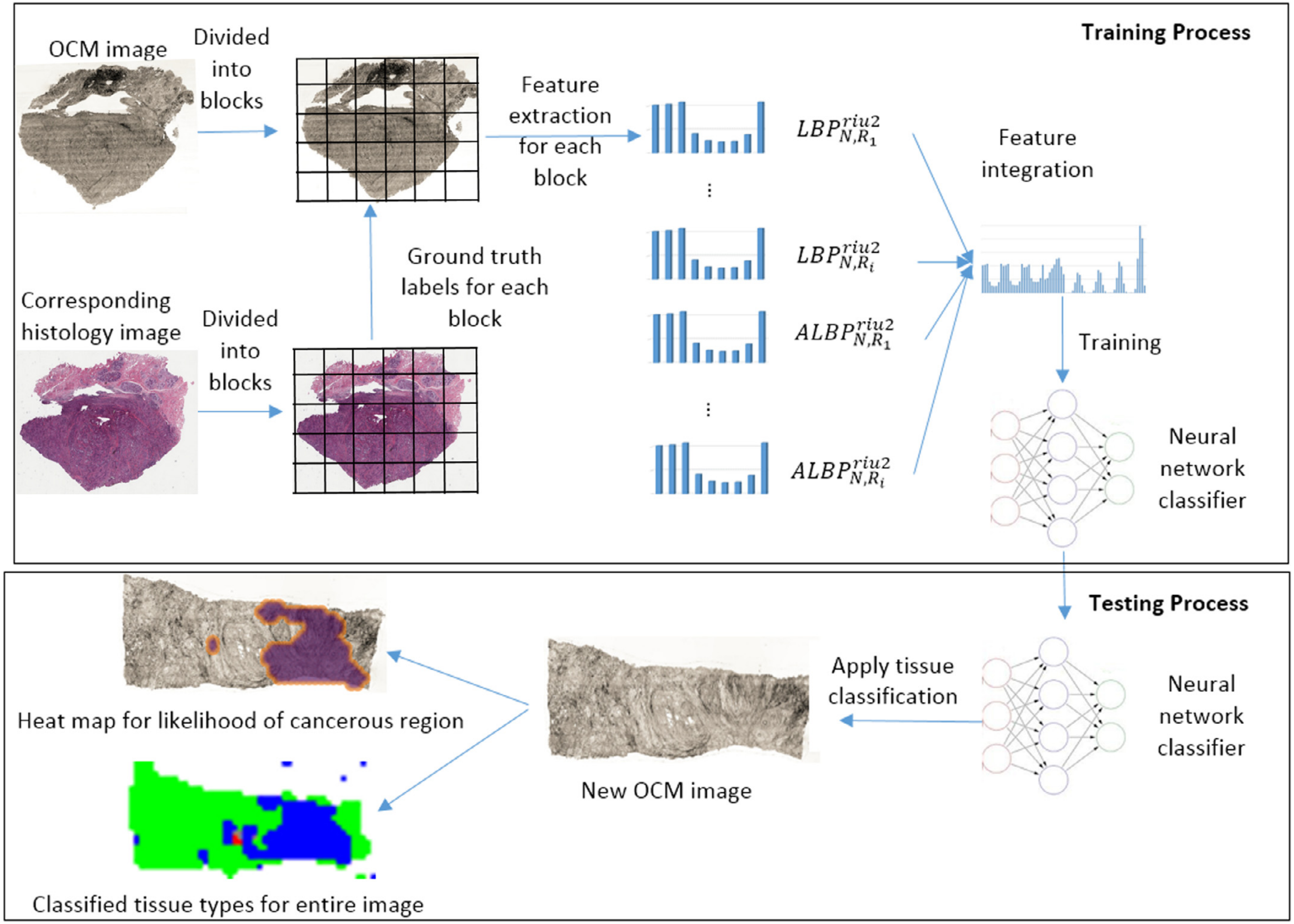

Wan, S., Lee, H. C., Huang, X., Xu, T., Xu, T., Zeng, X., ... & Zhou, C. (2017). Integrated local binary pattern texture features for classification of breast tissue imaged by optical coherence microscopy. Medical image analysis, 38, 104-116.

Deep image reconstruction from human brain activity

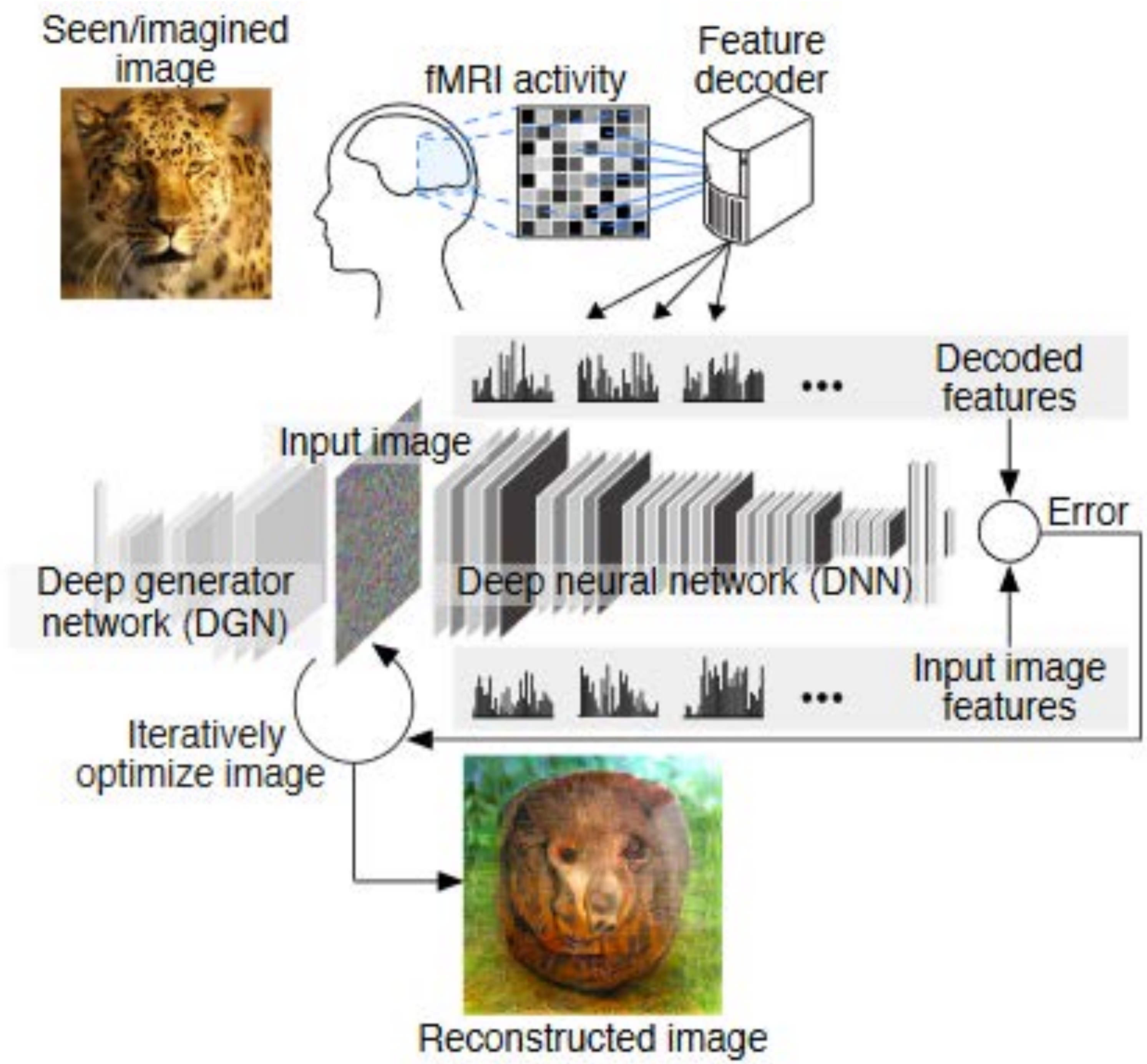

Overview of deep image reconstruction. The pixels' values of the input image are optimized so that the DNN features of the image are similar to those decoded from fMRI activity. A deep generator network (DGN) is optionally combined with the DNN to produce natural-looking images, in which optimization is performed at the input space of the DGN.

Shen, G., Horikawa, T., Majima, K., & Kamitani, Y. (2017). Deep image reconstruction from human brain activity. bioRxiv, 240317.

Predicting the sequence specificities of DNA- and RNA-binding proteins by deep learning

Babak Alipanahi[1,2,6], Andrew Delong[1,6], Matthew T Weirauch[3–5] & Brendan J Frey[1–3]

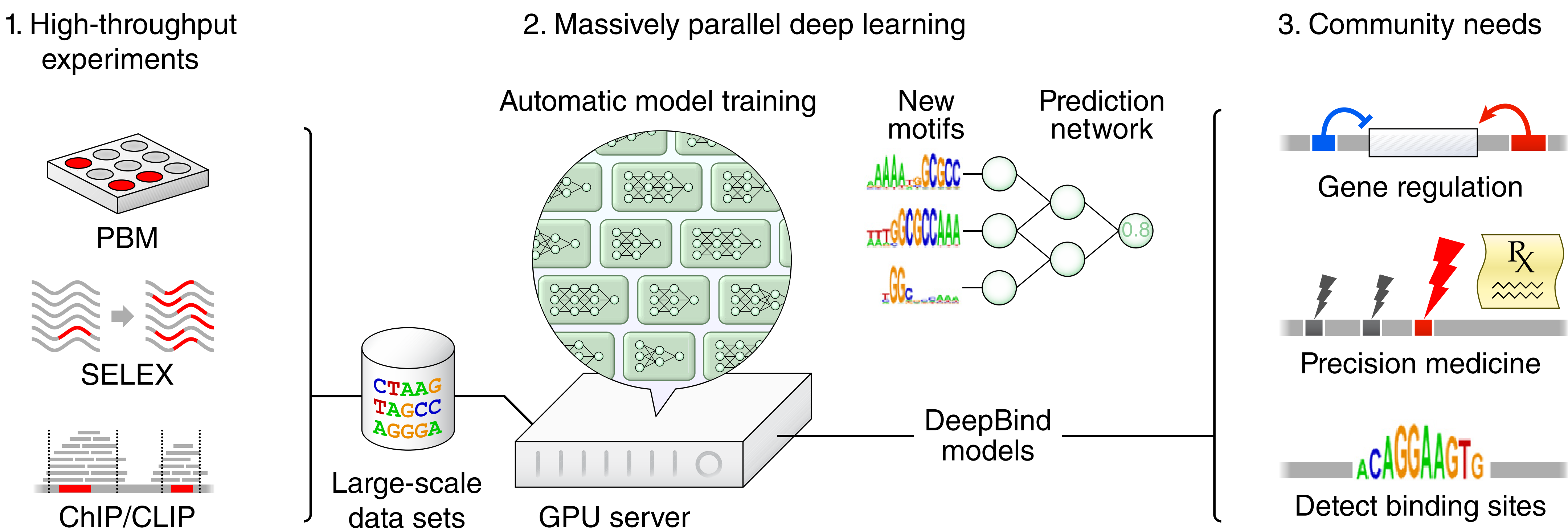

Figure 1 DeepBind's input data, training procedure and applications. 1. The sequence specificities of DNA- and RNA-binding proteins can now be measured by several types of high-throughput assay, including PBM, SELEX, and ChIP- and CLIP-seq techniques. 2. DeepBind captures these binding specificities from raw sequence data by jointly discovering new sequence motifs along with rules for combining them into a predictive binding score. Graphics processing units (GPUs) are used to automatically train high-quality models, with expert tuning allowed but not required. 3. The resulting DeepBind models can then be used to identify binding sites in test sequences and to score the effects of novel mutations.

Alipanahi, B., et. al. (2015). Predicting the sequence specificities of DNA-and RNA-binding proteins by deep learning. Nature biotechnology, 33(8), 831.

Improving optical microscopy

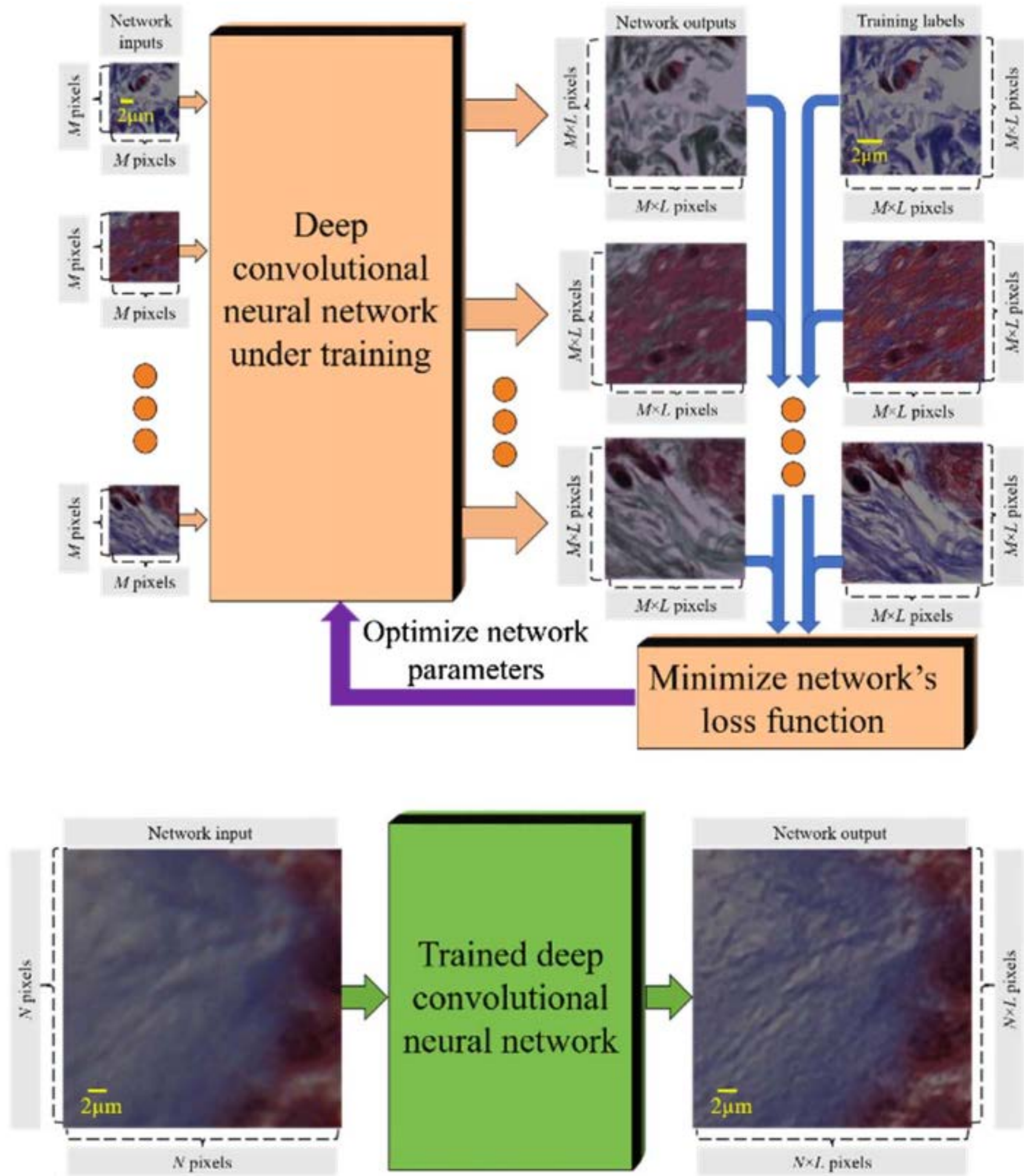

Rivenson, Y., Zhang, Y., Gunaydin, H., Teng, D., & Ozcan, A. (2017). Phase recovery and holographic image reconstruction using deep learning in neural networks. arXiv preprint arXiv:1705.04286.

Real-time detection of gravitational waves

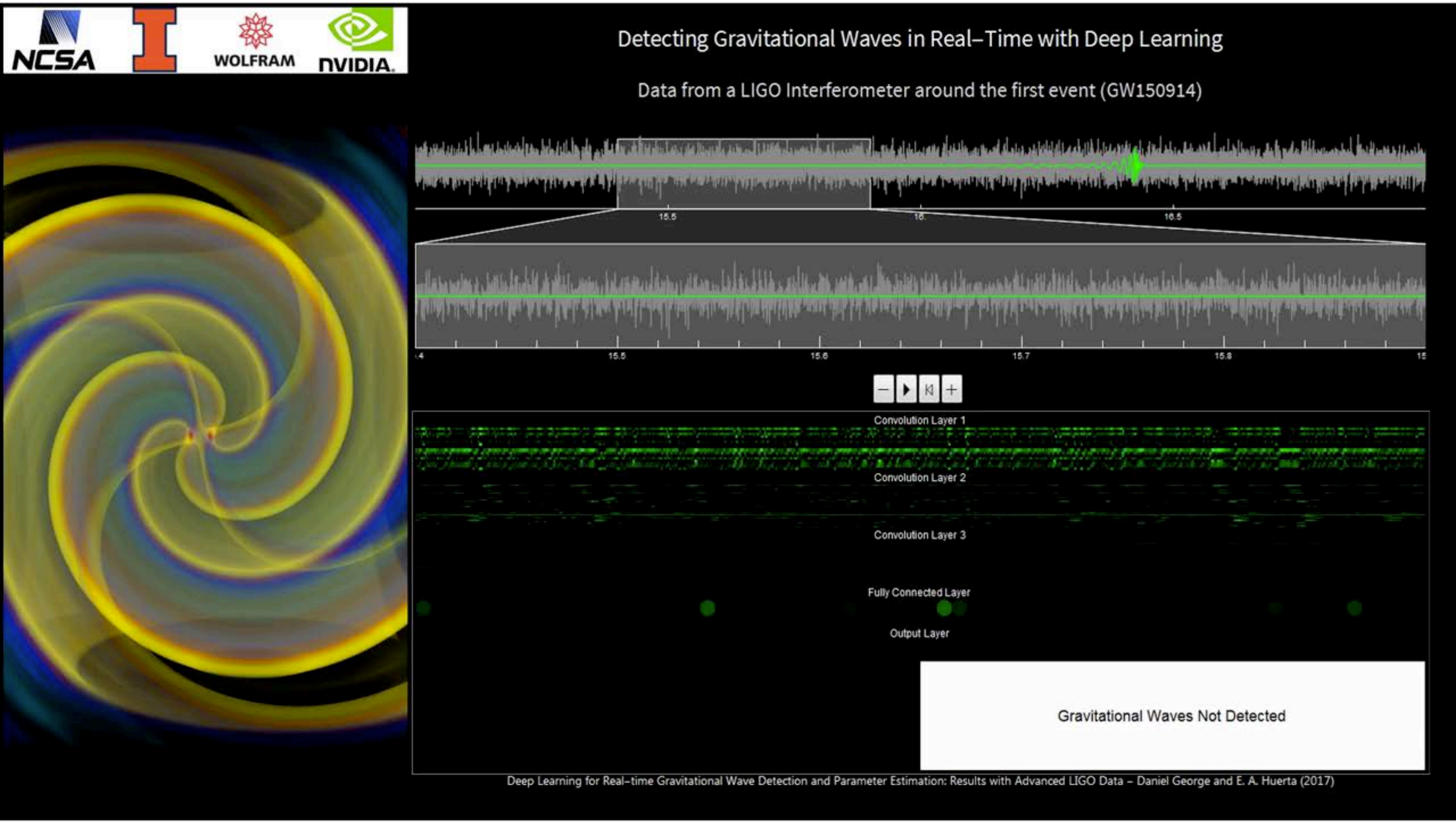

https://news.developer.nvidia.com/detecting-gravitational-waves-in-real-time-with-deep-learning/

Design of efficient molecular organic light-emitting diodes

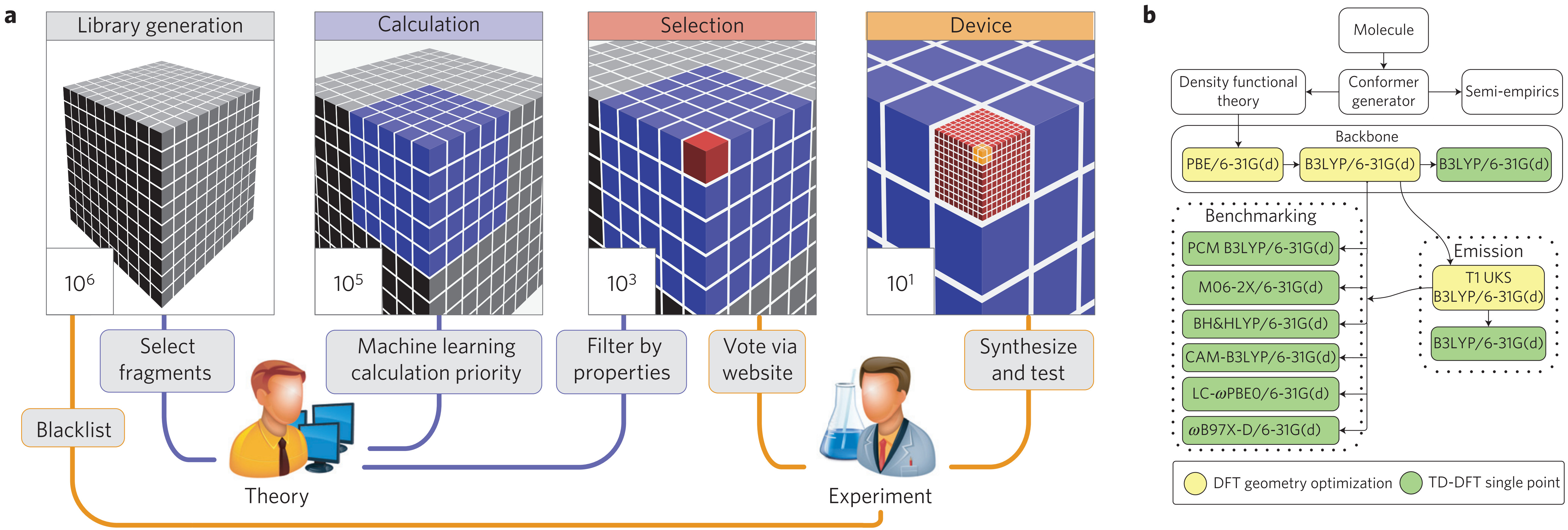

Figure 1 | Discovery pipeline. a, Diagram of the collaborative discovery approach: the search space decreases by over five orders of magnitude as the screening progresses. The cubes represent the size of the chemical space considered at any given stage of the process. The distinct screening stages, from left to right, involve different theoretical and computational approaches as well as experimental input and testing. **b**, Dependency tree for the quantum chemistry calculations employed in this study. The calculations labelled as backbone were performed for all analysed molecules, leading compounds were also characterized using the methods labelled emission, and the benchmarking calculations were used to assess predictive power.

Gómez-Bombarelli, R., Aguilera-Iparraguirre, J., Hirzel, T. D., Duvenaud, D., Maclaurin, D., Blood-Forsythe, M. A., ... & Markopoulos, G. (2016). Design of efficient molecular organic light-emitting diodes by a high-throughput virtual screening and experimental approach. Nature materials, 15(10), 1120.

Molecule design

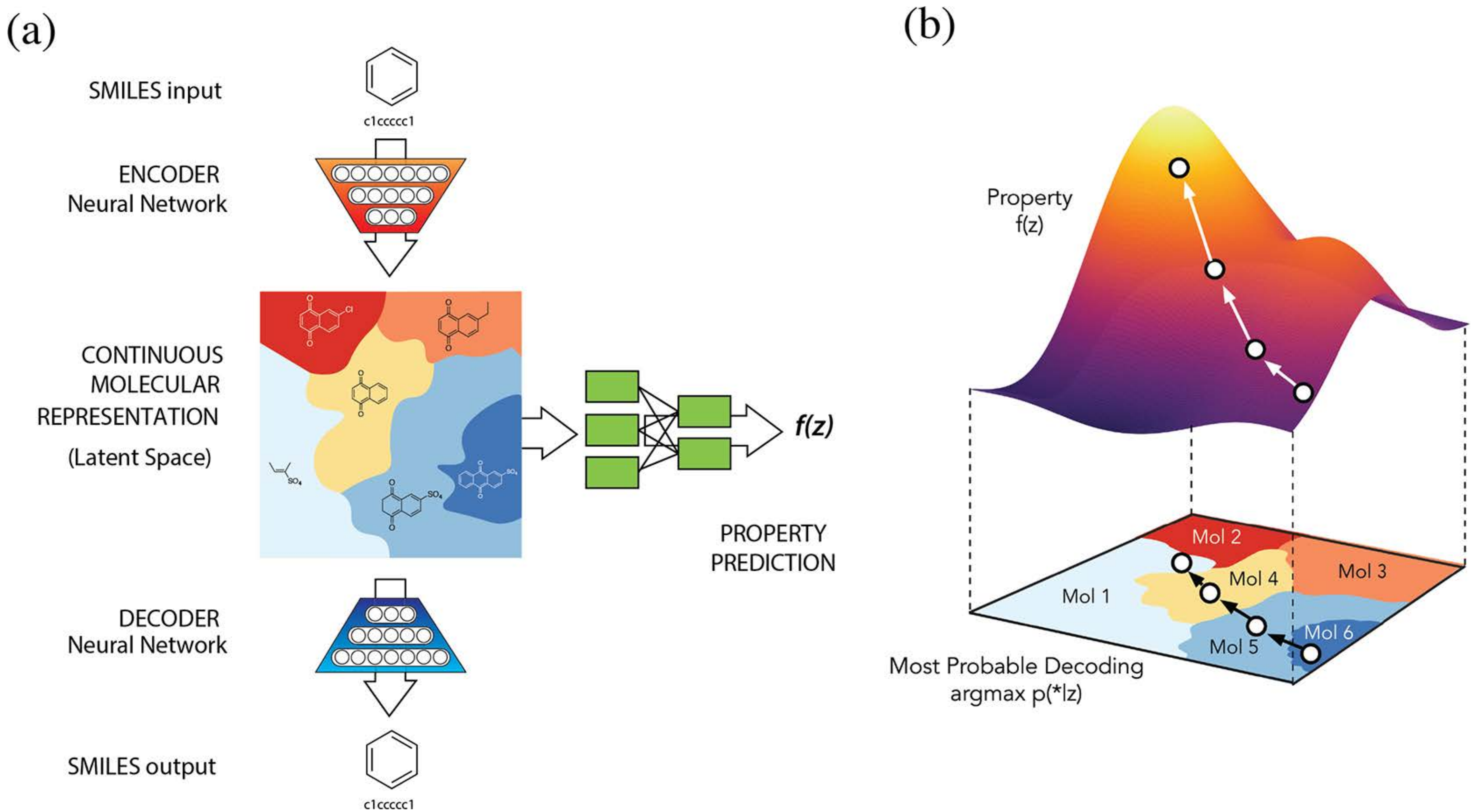

Figure 1. (a) A diagram of the autoencoder used for molecular design, including the joint property prediction model. Starting from a discrete molecular representation, such as a SMILES string, the encoder network converts each molecule into a vector in the latent space, which is effectively a continuous molecular representation. Given a point in the latent space, the decoder network produces a corresponding SMILES string. A mutilayer perceptron network estimates the value of target properties associated with each molecule. (b) Gradient-based optimization in continuous latent space. After training a surrogate model $f(z)$ to predict the properties of molecules based on their latent representation z, we can optimize $f(z)$ with respect to z to find new latent representations expected to have high values of desired properties. These new latent representations can then be decoded into SMILES strings, at which point their properties can be tested empirically.

Gómez-Bombarelli, R., Wei, J. N., Duvenaud, D., Hernández-Lobato, J. M., Sánchez-Lengeling, B., Sheberla, D., ... & Aspuru-Guzik, A. (2016). Automatic chemical design using a data-driven continuous representation of molecules. ACS Central Science.

Auto-tuning code for high-performance computing

```
def avgpool(float(B, C, H, W) input) -> (output) {{
    output(b, c, h, w) += input(b, c, h * {sH} + kh, w * {sW} + kw)
                          where kh in 0:{kH}, kw in 0:{kW}
}}
```

Tensor Comprehension for 2D Average Pooling

https://research.fb.com/announcing-tensor-comprehensions/

How certain are you about your machine learning model predictions?